E158 Liquid Hydrogen Target Milestone Report

R. W. Carr, J. Gao, C. E. Jones and R. D. McKeown
W. K. Kellogg Radiation Laboratory
California Institute of Technology

April 21, 1999

Contents

1 Milestones for the E158 Liquid Hydrogen Target

The EPAC subpanel for E158 milestones established one milestone regarding the E158 target for second stage approval: Evaluate target boiling. This milestone is meant to address the most important issue regarding the performance of the target for the E158 experiment, which is that the temperature, and hence density, of the liquid hydrogen in the beam path must be sufficiently stable that the contribution to the width of the asymmetry distribution from variation in the target thickness does not dominate the statistical uncertainty of the measurement. For each beam pulse, the Møller yield is to be measured with a fractional statistical precision of 2×10^{-4}. To avoid degradation of the precision of the measurement, the target is subject to the constraint on pulse-to-pulse density variation of $\delta\rho/\rho < 10^{-4}$.

The target density fluctuations on the timescale of the beam repetition rate arise from pulse-to-pulse variations in the energy deposited into the fluid by the beam ionizing the target atoms and pulse-to-pulse variations in the energy dissipated between beam pulses through mixing with colder fluid in the region outside the target−beam interaction volume. For a flux of 6×10^{11} (45 GeV) minimum ionizing particles per pulse through the 1.5 m long target, we have 490 Watts deposited into the fluid by the beam.

In this document, we address the milestone on two separate fronts. In section 4, we present the results of measurements made in 1998 of density fluctuations in the SAMPLE target and extrapolate to the expected performance with the SLAC electron beam. However, this is not sufficient to fully address the issue since the E158 and SAMPLE targets are not identical. Therefore, we start the report by presenting the design for the E158 target, then discuss its differences and similarities to the SAMPLE target and, in Section 3, describe the elements of the E158 target design that promote and maintain transverse flow and fluid mixing in the target region. In section 5 we discuss the magnitude of the density change due to beam heating that we expect to occur during a beam pulse and the heating of the fluid due to incomplete mixing between beam pulses. Based upon those numbers, we calculate the size of density fluctuations that we expect due to pulse-to-pulse variations in the beam intensity. In section 6 we follow the same procedure to estimate density fluctuations due to pulse-to-pulse variations in the beamspot size.

2 Cryogenic Loop

The E158 liquid hydrogen target will be a high flow-rate recirculating system, with the major components of the cryogenic loop being the target cell, a pump, a heat exchanger and a high power heater. The target system is designed based on the experience with the target used at the MIT/Bates accelerator for the SAMPLE parity violation experiment. Here we describe and contrast the SAMPLE and E158 targets.

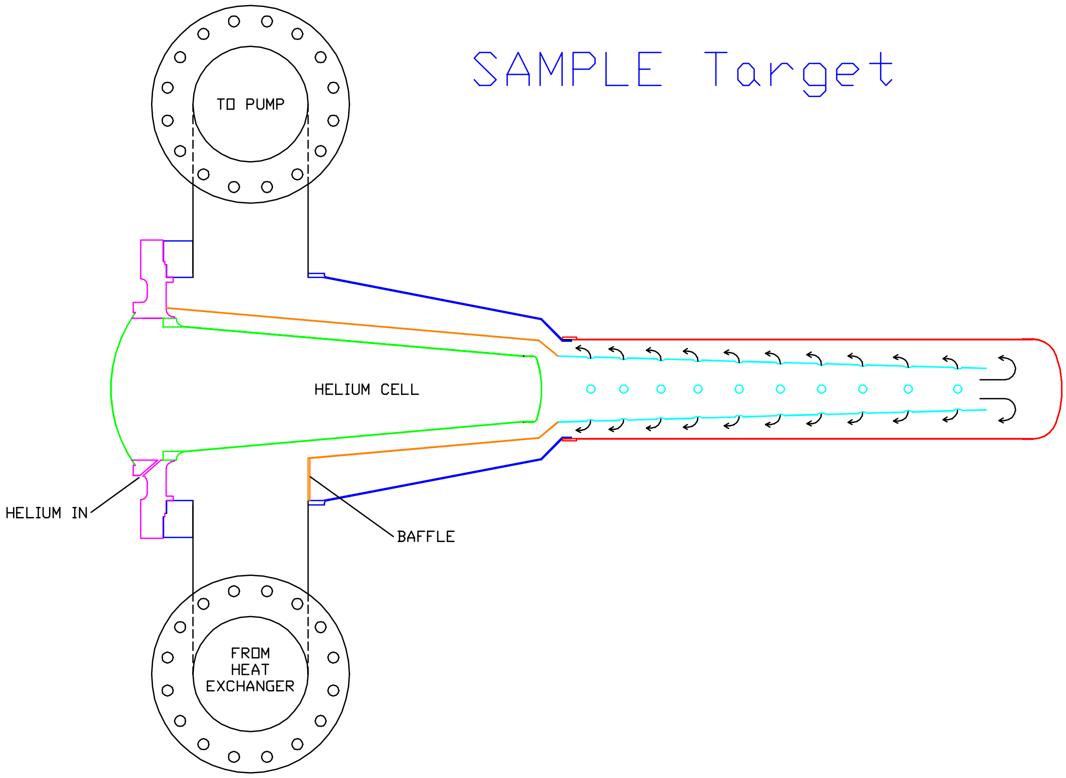

Figure 1: Schematic diagram of the SAMPLE hydrogen target cell, helium cell and flow manifold.

2.1 SAMPLE Target Design

The SAMPLE cryogenic loop is shown in figure 2, with a more detailed view of the target cell and manifold in figure 1. The electron beam enters the target through the end window on the hydrogen target cell opposite the helium cell and exits the target through the helium cell. The hydrogen target cell is 3" diameter and 40 cm long, and is backed by a helium cell to provide an exit window with the same curvature as the entrance window so that the target length is insensitive to small changes in the beam position. The liquid hydrogen enters the target region through a manifold off-center from the beam axis, flows down the length of the target region and back near the outside walls in the annulus formed by the outer wall of the cylindrical cell and a thin conical shell (the "windsock") that extends along the length of the target cell. The windsock terminates about 1" downstream of the entrance window to the hydrogen cell. It has small holes punched in the sides to promote transverse flow out of the target region along the length of the cell.

The SAMPLE cryogenic loop extends in the vertical direction with a vane-axial pump and heater on the outlet side of the target cell and a heat exchanger on the inlet side to the target region. The pump consists of impellers connected by a shaft to a 0.5 horsepower motor housed outside the vacuum volume. It is capable of moving the

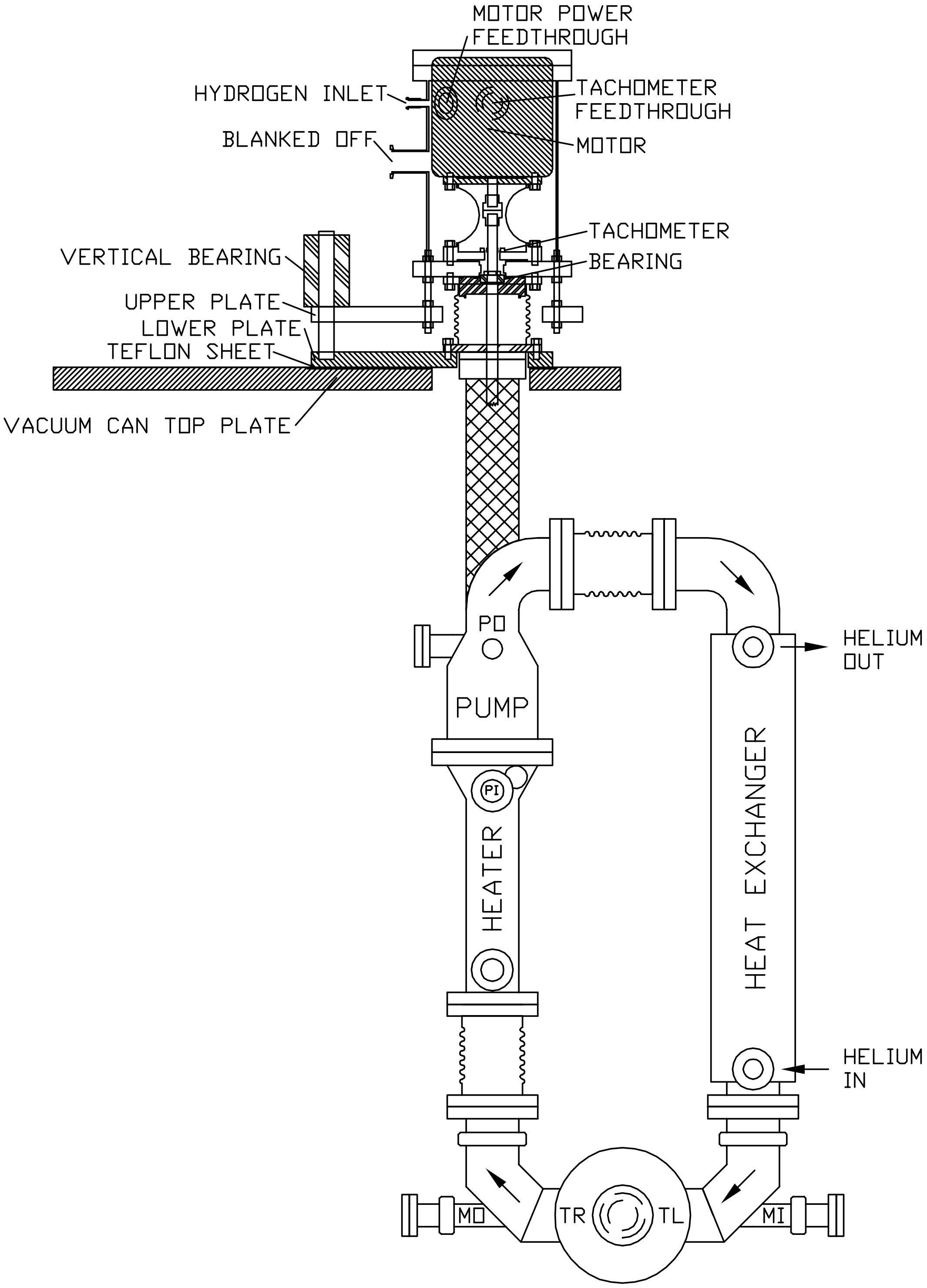

Figure 2: Schematic diagram of the SAMPLE liquid hydrogen cryotarget.

fluid at an average velocity of 7 m/s in the target region, with a velocity of 5 m/s at the entrance to the target region where the windsock is widest and 10 m/s at the narrow end of the windsock. The heat exchanger consists of a bronze bellows inside a vacuum jacket, with the coolant helium gas flowing between the bellows and the outside wall and the hydrogen flowing in the center, inside the bellows. The coolant is supplied at 12 K and mass flow rate 17 g/s by a refrigerator. The heat exchanger is designed as a counterflow device with the helium inlet at the end nearest the hydrogen exit to the heat exchanger. Normal operating parameters for the target are a liquid hydrogen temperature of 20 K and pressure of 25 psia.

In practice, we find that the SAMPLE heat exchanger and refrigerator can remove 750 W of power from the hydrogen. The SAMPLE target heat load is roughly 450 W from beam heating, 100 W from thermal leaks to the outside world, and 100 W from the pump heating the fluid. The loop contains a high power heater whose function is to maintain a constant heat load on the target. It is controlled in a feedback loop with a beam current monitor to compensate for large changes in the beam current. The temperature of the coolant returned to the refrigerator is held constant, in a feedback loop with a heater on the coolant supply line in the refrigerator. This prevents small fluctuations in the liquid hydrogen temperature but does not respond quickly enough to compensate for a loss of beam.

2.2 E158 Target Design

A schematic view of the E158 target is shown in figure 3. The target cell is a cylinder 1.5 meters long by 3" in diameter and is fronted by a helium cell. The beam enters through the helium cell, and the liquid hydrogen enters the target cell end opposite the helium cell. The target cell occupies one side of the cryogenic loop. The rest of the loop consists of a vane-axial pump, a counterflow heat exchanger, a heater and the plumbing connecting the different elements. The pump will be a scaled version of the SAMPLE pump, designed to provide a liquid hydrogen longitudinal speed of 7 m/s in the target cell. The heat exchanger will follow the design of the SAMPLE heat exchanger, being a bellows-type device with counterflow of the hydrogen and coolant. The heat exchanger for SAMPLE was designed to remove 850 W from the hydrogen, and its performance appears to be limited by the refrigerator. We will design the heat exchanger for E158 to remove 1000 W of power and request that SLAC provide a refrigerator with the same capacity. The heat budget for the E158 target is 500 W from the beam, 100 W from heat leaks through the target supports and 200 W from pumping the fluid. There will be a heater in the target loop to serve the same function as that in the SAMPLE target.

Although the volume of the E158 target will not be known until a detailed design with machine drawings is completed, we estimate that it will be ~ 60 liters, as compared to the 25 liter SAMPLE target volume. We have increased the heat budget for moving the fluid because of the extra mass in the E158 target and because we are introducing new features into the target region to reduce density fluctuations that will increase

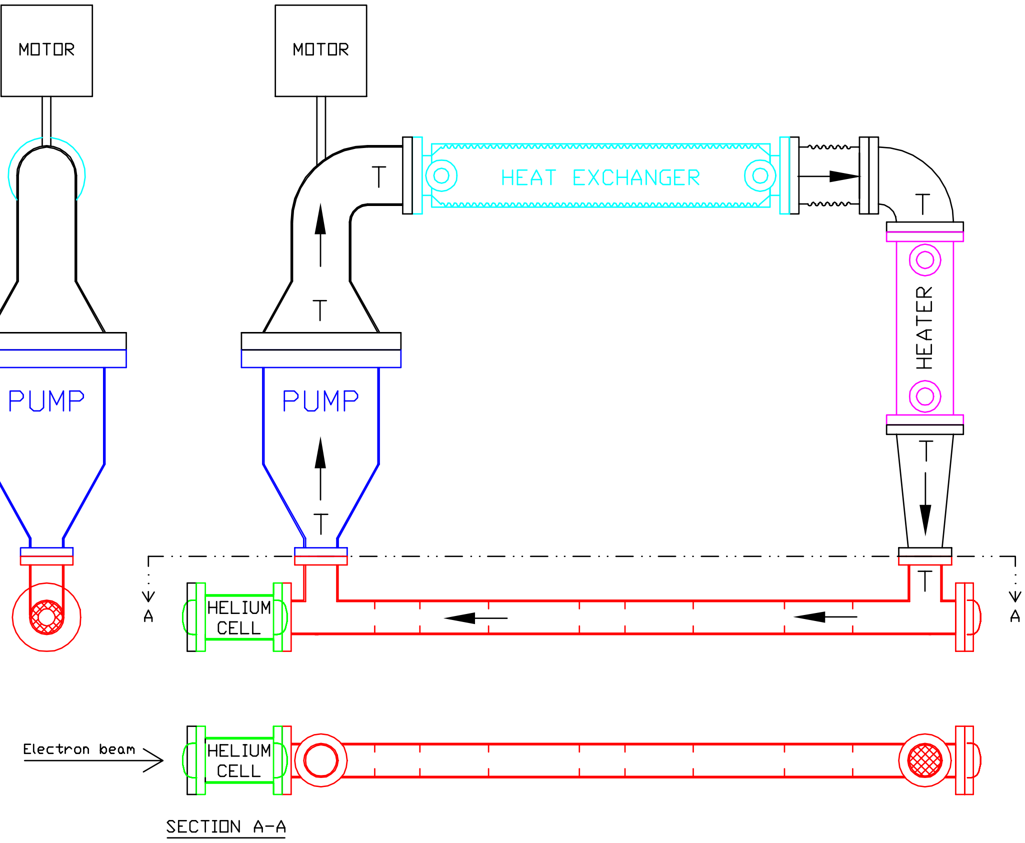

Figure 3: Schematic diagram of the E158 liquid hydrogen cryotarget.

the impedance to flow. Those elements will be described in detail in section 3.

The major difference between the E158 target and the SAMPLE target is the size of the target cell. The SAMPLE target length is 40 cm, while the E158 target length is 150 cm. The obvious first choice of simply scaling the SAMPLE target for the E158 experiment does not work for several reasons. The SAMPLE target is 7.6 cm wide, so scaling the SAMPLE target cell to 150 cm length would require a cell width of 29 cm, or a volume of nearly 100 liters in the target cell alone. The pump, heat exchanger and tubing diameter in the rest of the loop would have to be scaled in size by roughly a factor of four. This would lead to a prohibitively large volume of hydrogen for the target. Furthermore, it is not clear that the devices that introduce transverse flow and mixing in the SAMPLE target would work adequately for the longer target in the E158 experiment. Fortunately, scaling directly from the SAMPLE target is unnecessary because there are other ways to get mixing in the E158 target that do not require the large volume and which should work better than the SAMPLE target design. Those are described in the next section.

3 Transverse Flow and Mixing in the Target Region

The fluid flow can be described in terms of a large-scale laminar-like flow that describes the average velocity of the whole fluid and turbulent flow that introduces local velocity differences that vary from place to place within the fluid volume. At any given point, the net flow is a superposition of the bulk flow and the turbulent flow.

In order to reduce density variations that can arise from beam heating of the liquid hydrogen, it is necessary to move the fluid heated by a beam pulse out of the beam volume, replacing it with cold fluid from outside in the time between pulses. There are two things that can be done to facilitate this. The first is to design the target so that the average flow in the target region has a transverse component that moves the heated hydrogen away from the beam axis quickly enough that the fluid is replaced in the interaction region between pulses. The second is to promote turbulence which mixes the fluid. The Reynolds number for the fluid flowing through the 3" diameter target cell is quite high, 10^6, so the flow will tend to be turbulent in any case, but the size of the vortices of the turbulent flow will not necessarily be optimal for the kind of mixing that is needed. In practice, it is necessary to promote and maintain turbulence of the right scale to mix new fluid into the interaction region. The correct scale for this turbulence is of order the beam diameter, since turbulence of a much smaller scale will not move unheated fluid into the interaction volume and turbulence of a much larger scale could mix the fluid too slowly for it to be replaced between beam pulses at our pumping speed.

For the E158 cryotarget, we incorporated structures into the target region that both introduce a transverse component to the bulk flow and promote turbulence of the scale of ~ 2 mm, i.e., roughly the size of the beam. There is a geometric constraint on the target cell from the requirement that no material other than hydrogen be within 10 beam radii of the center and no two-scattering beam background events be within the detector acceptance. This translates into the practical limits that no material other than the hydrogen can be within 0.75" (19 mm) of the beam axis and any material in the region $0.75'' < r < 1.5''$ be thin compared to the hydrogen in that region. We propose inserting a series of discs made of aluminum wire mesh into the target cell. We chose aluminum because it is nonmagnetic, of low density, and does not activate as much as copper in the radiation environment. The discs are oriented perpendicular to the beam axis and have a 1.5" diameter hole cut out of the center to provide the clearance around the beam axis. In addition, each disc has an open slot that covers 45° of angular range around the outside. A schematic drawing of four successive discs is shown in figure 4. The second disc has the slot diametrically opposed to the first, the third disc's slot is opposite the second but offset by 45°, the fourth is diametrically opposed to the third disc's slot, and so on. This way the slots introduce the large scale transverse motion to the flow, while flow through the mesh introduces the small scale turbulence which is reestablished as the fluid passes

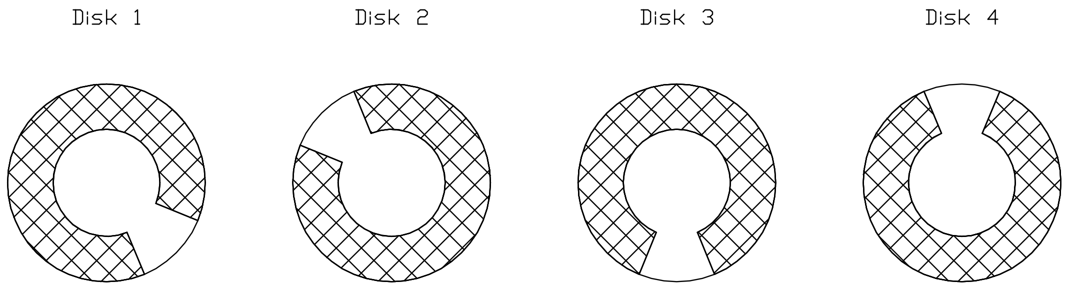

Figure 4: View of four successive discs, showing the relative orientations of the slots that introduce a transverse velocity component to the average fluid flow.

through the mesh at each disc.

The mesh parameters that are fine-tuned to provide the flow that we want are the disc spacing (large scale transverse motion) and the wire diameter and mesh opening (turbulence). The disc spacing was chosen randomly in the range $6'' \pm 2''$. The spacing is not periodic so that we avoid resonances that might move a packet of fluid into the interaction region in phase with the beam pulses. The average spacing of 6" was chosen such that the transverse velocity moves the fluid 4 mm between beam pulses. Eight discs are inserted into the target region so that the integrated added material is the same at all azimuthal angles about the beam axis.

The turbulence is established and maintained by the series of wire mesh discs. While flow through a wire mesh has not been well quantified by the fluid dynamics community because of its complexity, several general features are known which are sufficient for what we need to do. In particular, it is known that a wire mesh introduces turbulence of two scales, one being the wire diameter and the other being the spacing between wires. Turbulence of the latter scale arises because the turbulent vortices of the scale of the wires tend to join together at the points where the wires cross, forming the vortices the size of the opening. We have found aluminum wire mesh of two sizes that are reasonable; mesh count 6×6 with wire diameter 0.89 mm, opening 3.35 mm and mesh count 8×8 with wire diameter 0.71 mm, opening 2.46 mm. We have selected the 6×6 mesh because it will introduce turbulence of a slightly larger scale, which should mix unheated liquid hydrogen into the beam volume more thoroughly and will be better if we have to go to larger beam diameter. We note, however, that either mesh should work fine for the E158 target.

Practical design considerations that we encountered in coming up with this design were numerous. A few are delineated here because they are instructive in understanding why we think that the design that we chose is optimal.

1. An alternative design to introduce a transverse component to the flow is to cause the fluid to spiral down the target cell. This is not a good idea because to first order the fluid in the center does not move. In fact, rotational flow tends to stabilize the center, so it becomes *more* difficult to move fluid away from

the beam axis if it is the center of the tube. To make this into a useful device one needs to move the beam axis off center from the axis of the cylindrical target cell, with a significant displacement of the two axes necessary to have substantial transverse flow at the beam interaction region. This option would substantially increase the volume of the target, requiring a much larger pump and more hydrogen. Our design has the flow going back and forth across the cell, with a slow rotation of the transverse flow direction as the fluid goes through the cell. We plan to avoid any design feature that would introduce rotational flow.

2. One could use a solid disc instead of a screen, but this has three disadvantages. Firstly, the liquid hydrogen could cavitate behind the solid disc causing unpredictable variations in the target density. This could be avoided by tilting the disc axis relative to the axis of the target cell, but most solutions of this kind tend to introduce rotational flow which would have to be prevented with some new device in the target region. Secondly, the pressure drop across a solid plate is larger than the pressure drop across a mesh of the same solidity, so using solid plates would lead to an overall reduction in the flow velocity. Lastly, the solid plate doesn't introduce the small scale turbulence, only turbulence of the size of the opening in the plate.

3. An optimal design requires that there be turbulent vortices of diameter approximately the beam diameter in the target region. The most straightforward way to achieve this is to put wires of $\sim 1-2$ mm diameter near the beam volume. However, nothing can be placed within 0.75" of the beam axis. Alternatively, one could place the wires across the inlet to the target cell, but the turbulence is not guaranteed to remain the scale of the wire throughout the 1.5 m target length. Putting screens in along the length of the target cell will generate the turbulence and maintain it throughout the length of the target.

4. The amount of material introduced into the target cell in the region $0.75'' < r < 1.5''$ should be small since some secondary scattering can occur. The 6×6 mesh is about 20% heavier than the 8×8 mesh, yet still only adds 0.67 g/cm^2 of material to the outer part of the target cell. The hydrogen thickness in that region is 10.5 g/cm^2.

In the SAMPLE target, the only part that explicitly promotes turbulence of $1-2$ mm size are the holes in the windsock, which primarily affects the flow leaving the target region and is not guaranteed to persist throughout the rest of the loop so that the flow coming into the target has this scale of turbulence. In fact the SAMPLE cryoloop is designed to minimize flow resistance due to turbulence and could damp out the turbulence of the needed scale. The bulk transverse flow in the SAMPLE target region comes from the fluid entering the target cell off-center, which is insufficient for full mixing to occur between beam pulses without turbulence of the right scale. The manifold for SAMPLE should introduce turbulence of the scale of ~ 10 mm, which is not optimal for the beam size.

4 Experience with the SAMPLE Target

The SAMPLE experiment serves as a good testing ground for E158 because many of the conditions for the two experiments are similar. The SAMPLE target is 40 cm long and the Bates beam is 40 μA, corresponding to a average heat load of about 450 Watts, while we expect 490 W of deposited energy for the SLAC beam. Both beams are pulsed, and the number of incident electrons per pulse is about the same (5×10^{11} at Bates, 6×10^{11} at SLAC). The timescale of the beam pulse length (250 ns at SLAC and 15$-$25 μsec at Bates) is short compared to the time between pulses at both accelerators. The radius of the beam at Bates was $r_b = 1.3$ mm (1σ) in the 1998 run, compared to the SLAC beam radius of $r_b = 1-2$ mm. Therefore, the energy per unit volume deposited in the liquid is roughly comparable for the SAMPLE case and for E158, with less energy deposited on average per unit volume in the E158 target (approximately 40% for $r_b = 1$ mm at SLAC).

A significant difference involves the pulse rate. At Bates the pulse rate is 600 Hz compared to 120 Hz for E158. This implies that there is five times as much time for thermal mixing between pulses at SLAC. The Reynolds number for the flow in the target region is high, $\sim 10^6$, for both experiments, so we expect that the flow is turbulent and there is substantial mixing with surrounding fluid between beam pulses. In the E158 target we will promote turbulence of the right scale to efficiently mix new fluid into the beam volume.

The timescale for the hydrogen density to change due to energy deposited by the beam, i.e. the timescale of thermal expansion, is set by the velocity of sound in liquid hydrogen, which is $v_s = 1.1 \times 10^6$ mm/s at our operating temperature and pressure. The beam pulse duration is sufficiently long at both SLAC and Bates that we expect the density to change during the pulse. The magnitude of the density change and its effect on the counting statistics are calculated in section 5. The shorter pulse length at SLAC (250 ns) leads to a smaller effect for E158 than for the SAMPLE experiment.

The thermal stability properties of SAMPLE target have been investigated previously and reported in Beise *et al*, Nucl. Instrum. Methods **A378**, 383 (1996); we have subsequently studied the performance in greater detail during a SAMPLE experiment production run in summer 1998. We study the SAMPLE target as a function of pulse rate, so it is straightforward to extract the expected performance for SLAC beam conditions from the SAMPLE studies.

During the 1998 SAMPLE run, we implemented forward angle "luminosity monitors" in order to study target boiling effects with greater sensitivity and to test our ability to measure small asymmetries. These monitors were lucite Cerenkov detectors coupled to photomultipliers. The integrated charge was read out for every beam pulse and normalized to the incident charge (measured with a beam toroid monitor) for that pulse. Data from pulse pairs separated by 1/60 second were combined to form an asymmetry (difference of lumi/toroid ratios over the sum). When compiled into a histogram, the asymmetries average to zero and there is a finite width (presumably dominated by counting statistics in the lumi monitor) to the gaussian distribution that is sensitive to target density changes. The fractional lumi asymmetry width (in percent) is plotted in figure 5 as a function of the beam pulse rate in Hz. All ten timeslots (pulses synched to a 60 Hz reference) were analyzed separately. Shown in figure 5 are the data for timeslot 1 (the worst) and timeslot 5 (typical). It is not known whether the difference between the two timeslots is due to electronic noise in the first timeslot or a real change in the physical parameters of the beam, such as the shape.

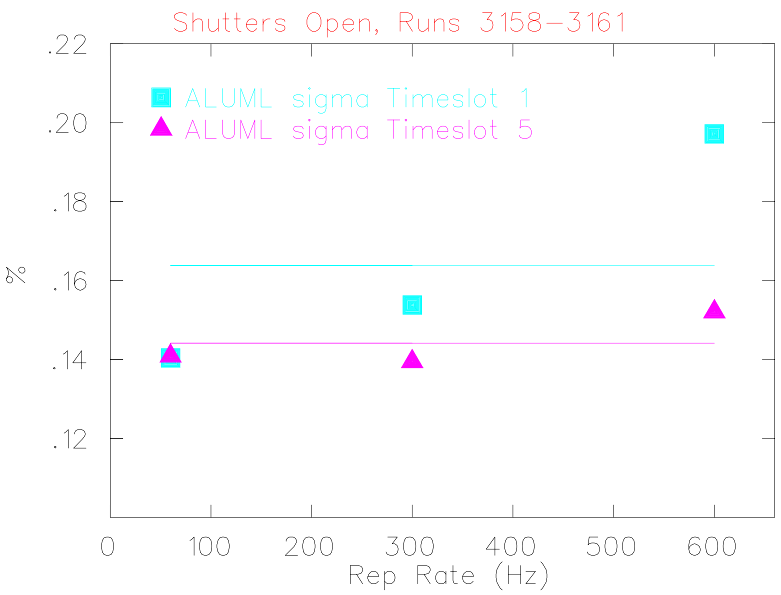

Figure 5: Target boiling study data from the SAMPLE experiment

From figure 5 one sees that the width of the lumi asymmetry distribution increases with beam repetition rate. This is a signal that the target density is changed by the energy deposited by the beam. The experimental data shows that growth of the width of the asymmetry distribution appears to be quadratic of the form

$$\Sigma(\%) = \Sigma_0(\%) + \alpha \times (\mathrm{reprate})^2 \,.$$

For the two timeslots, we can determine the values of α to be 1.7×10^{-7} and 4.4×10^{-8} and $\Sigma_0 = 0.14\%$. Thus, at the value of 120 Hz relevant to E158 we would have the fractional widths $\Sigma(120) = \Sigma_0 + 2.4 \times 10^{-3}$ % and $\Sigma(120) = \Sigma_0 + 6.4 \times 10^{-4}$ %. For a given reprate the target density fluctuations add quadratically with the other statistical fluctuations. Therefore, we expect

$$\Sigma(120) = [(\Sigma_0)^2 + (\Sigma_t)^2]^{1/2}$$

where Σ_t is the target boiling contribution. Using the data above, we then can extract the two values of Σ_t to be $2.6 \times 10^{-2}\%$ and $1.3 \times 10^{-2}\%$. These numbers are comparable to the E158 statistical precision of $2 \times 10^{-2}\%$ for one beam pulse.

Under these conditions the SAMPLE target density fluctuations are non-negligible compared to the counting statistics of the Møller scattering measurement.

We note that when the SAMPLE boiling study was performed the SAMPLE target was not operating optimally. Indeed, the target was running only 0.5 K sub-cooled. The target normally runs $1.5 - 2.0$ K sub-cooled, but after many weeks of running the pressures and temperatures varied somewhat. Since the performance was adequate for SAMPLE, data acquisition was not interrupted to address this issue.

5 Density Fluctuations due to Beam Intensity Variation

5.1 Density Change During the Beam Pulse

In principle, one would expect the density of the liquid hydrogen in the beam volume to change as energy is deposited into it on a timescale set by the speed of sound in the fluid. For liquid hydrogen at 20 K and 2 atm, the speed at which the thermal expansion propagates is 1.1×10^{-3} mm/ns. We modeled the effective loss of fluid from the beam volume during the pulse assuming a spatially uniform beam of radius r_b and linear time dependence of the instantaneous current of the form

$$i(t) = i_{ave}\left[c_1 + c_2\frac{t}{\tau}\right],$$

where τ is the pulse length. We assume that the peak current is highest at the start of the pulse and that the current decreases by $\sim 20\%$ by the end of the pulse ($c_1 = 1.1$ and $c_2 = -0.2$). The model assumes there is no mixing during the pulse, which is an excellent approximation for our flow velocity of 7 m/s. The loss of mass from the beam volume, which we refer to as the effective density reduction, is weighted by the beam current because the observed quantity is the counting statistics which depends upon the product of the number of target atoms and the beam current.

We estimate that for $\tau = 370$ ns and $N_e = i_{ave}\tau = 6 \times 10^{11}$ e$^-$ per pulse the beam-weighted average effective density reduction during the beam pulse is $\Delta\rho/\rho = -0.24\%$ for $r_b = 1$ mm, $\Delta\rho/\rho = -0.032\%$ for $r_b = 2$ mm, and $\Delta\rho/\rho = -0.010\%$ for $r_b = 3$ mm. This small decrease will not affect the counting statistics of the experiment.

Because of the expansion during the beam pulse, one can get pulse-to-pulse density fluctuations that arise from pulse-to-pulse changes in the beam intensity. We calculate that beam intensity fluctuations of $\Delta I/I = 1\%$ give rise to density fluctuation of $\delta\rho/\rho = 2.4 \times 10^{-5}$ for a 1 mm beam spot, $\delta\rho/\rho = 3.2 \times 10^{-6}$ for a 2 mm beam spot, and $\delta\rho/\rho = 1.0 \times 10^{-6}$ for a 3 mm beam spot. These are significantly below our goal of 10^{-4}. The values for the 48 MeV beam parameters of $N_e = 4 \times 10^{11}$ e$^-$/pulse and $\tau = 250$ ns are even smaller.

We studied the effect of changes in the time structure of the beam pulse on the target density and found it to be negligible for a reasonable range of pulse time structures with the same total number of electrons in the pulse.

5.2 Fluid Mixing Between Beam Pulses

In this section we estimate the effect of mixing between pulses on the density of the liquid hydrogen in the target region.

Between beam pulses the heated fluid in the beam path is moved off axis by approximately 4 mm on average (see section 3) and mixed through turbulence with the surrounding, unheated fluid. We have estimated the effect of incomplete mixing on the density of the fluid in beam path when the next beam pulse arrives, assuming that the fluid in the beam path is uniformly mixed with the unheated fluid around the beam in a volume of radius $r_{beam} + (N/2) * r_{turb}$. r_{turb} is the radius of the turbulent vortices, taken to be the spacing of the wire mesh, and N is the estimated number of vortices in which a fluid packet mixes completely between pulses (3 for our flow conditions). Given these assumptions and the estimate for the density change from beam heating, we find that the density of fluid in the beam path at the time the second pulse arrives is reduced by $\sim 2 - 4 \times 10^{-4}$ relative to unheated fluid. These numbers are valid for both the 45 GeV beam structure (6×10^{11} e$^-$/pulse and $\tau = 370$ ns) or the 48 GeV beam structure (4×10^{11} e$^-$/pulse and $\tau = 250$ ns), with the lower currents corresponding to the lower end of the limits. Assuming that the fluid stays in the target region for 26 consecutive pulses, the density of fluid in the beam path near the exit of the target cell is decreased by $\lesssim 1\%$ relative to that of fluid entering the target region.

Based upon the estimate of the efficiency of mixing between pulses, we can infer that density fluctuations that occur during the pulse (see section 5.1) are reduced by one order of magnitude through mixing between pulses.

If the mixing is not the same from pulse to pulse, then it can introduce density fluctuations of its own. In the absence of external perturbations on the fluid, the mixing structures should be very stable in size and time evolution, with average fluctuations below the 1% level. In fact there will be some perturbations from vibrations of the liquid hydrogen pump, the support mechanism, etc. which are difficult to predict. In the absence of information, I assume that the diameter of the vortices in which the fluid mixes can vary by $\pm 5\%$, and find that the density fluctuations that arise from mixing are $\sim 1 - 3 \times 10^{-5}$.

The estimation of the mixing volume that the fluid occupies between pulses is crude and would benefit from experimental data about the flow downstream of the screens. Although we have tried to make conservative assumptions, these numbers for the density changes and fluctuations are best checked experimentally with the actual target.

r_{beam} (mm)	$\frac{\Delta r_{beam}}{r_{beam}}$	$\frac{\Delta\rho}{\rho}$
1.5	5%	-1.2×10^{-4} $+1.0 \times 10^{-4}$
1.5	10%	-2.7×10^{-4} $+1.8 \times 10^{-4}$
2.0	5%	-5×10^{-5} $+4 \times 10^{-5}$
2.0	10%	-1.2×10^{-4} $+0.8 \times 10^{-4}$
3.0	5%	-1.5×10^{-5} $+1.3 \times 10^{-5}$
3.0	10%	-3.5×10^{-5} $+2.4 \times 10^{-5}$

Table 1: Statistical fluctuation in the target density $\frac{\Delta\rho}{\rho}$ as a function of beam radius r_{beam} and percent jitter in the beam radius $\frac{\Delta r_{beam}}{r_{beam}}$ for $N_e = 6 \times 10^{11}$ and $\tau = 370$ ns.

r_{beam} (mm)	$\frac{\Delta r_{beam}}{r_{beam}}$	$\frac{\Delta\rho}{\rho}$
1.5	5%	-6×10^{-5} $+5 \times 10^{-5}$
1.5	10%	-1.3×10^{-4} $+0.8 \times 10^{-4}$
2.0	5%	-2.4×10^{-5} $+2.0 \times 10^{-5}$
2.0	10%	-5×10^{-5} $+4 \times 10^{-5}$
3.0	5%	-7×10^{-5} $+6 \times 10^{-6}$
3.0	10%	-1.6×10^{-5} $+1.1 \times 10^{-5}$

Table 2: Statistical fluctuation in the target density $\frac{\Delta\rho}{\rho}$ as a function of beam radius r_{beam} and percent jitter in the beam radius $\frac{\Delta r_{beam}}{r_{beam}}$ for $N_e = 4 \times 10^{11}$ and $\tau = 250$ ns.

6 Density Fluctuations due to Beam Size Variation

An estimate of the effect of fluctuations of the beam size on the target density during the beam pulse was made following the procedure used for beam intensity fluctuations outlined in section 5.1. A number of assumptions were made in this calculation because detailed information about fluctuations in the beam shape and size is limited at present. For instance, only the spotsize jitter in the vertical direction has been measured, and it was found to be approximately 10%. Based upon that information, we made the following assumptions in the calculations:

1. The beam is circular in cross section and the charge is distributed uniformly throughout the spot.
2. The changes in the beam size in the horizontal and vertical directions are always equal in magnitude, i.e., the beam remains circular.

The results of the calculations for beam radii of $r_{beam} = 1.5 - 3.0$ mm are shown in table 1 for the 45 GeV beam ($N_e = 6 \times 10^{11}$ e$^-$/pulse, $\tau = 370$ ns) and table 2 for the

48 GeV beam ($N_e = 4 \times 10^{11}$ e$^-$/pulse, $\tau = 250$ ns). Note that the effect is nonlinear, with a fluctuation to smaller radii introducing a larger change in the target density than a fluctuation of equal magnitude to larger radii.

The effect of changes in the beam size is significant; they cause the largest fluctuations in the target density of any effect considered in this report. Note that this calculation is for density changes occuring *during* the beam pulse, and hence changes to the geometry or flow to further improve mixing between pulses will not alter these fluctuations.

If the size jitter is 10%, then even a beam radius of 2 mm is too small to keep uncorrelated pulse-to-pulse density changes from dominating the statistical uncertainty if we use $N_e = 6 \times 10^{11}$ and 370 ns pulse length.

7 Conclusions

The above analysis indicates that a scaled version of the SAMPLE target would perform with density fluctuations that are marginal for the E158 required specification of 0.01% per beam pulse. For the E158 target, we have implemented a totally new technique for mixing the liquid hydrogen between beam pulses that is based upon extensive discussions with fluid flow experts from Caltech. These should substantially improve the mixing of fluid in the target−beam interaction region between pulses and therefore should give better density stability in the E158 target. Additionally, it will be very important to maintain optimal refrigerator and pump performance during E158 due to the more stringent requirements on target density fluctuations.

The density fluctuations arising from pulse-to-pulse variations in the intensity that occur during the beam pulse or through incomplete mixing between pulses do not pose a problem for the Møller experiment. By far the most serious source of density fluctuations is the beamspot size jitter. Because the estimates reported here show that they are potentially a serious problem, it will be necessary to measure their size with the target in the SLAC beam. We will then be able to vary the beam size, peak current and pulse length to reduce them.